

A Luminescent $[\text{Ru}_8\text{Pd}_4]^{24+}$ Supramolecular Cage

Diego Rota Martir,^a David B Cordes,^a Alexandra M. Z. Slawin,^a Daniel Escudero,^b Denis

Jacquemin,^b Stuart L. Warriner,^c and Eli Zysman-Colman^{a}*

^aOrganic Semiconductor Centre, EaStCHEM School of Chemistry, University of St Andrews, St Andrews, Fife, KY16 9ST, UK, Fax: +44-1334 463808; Tel: +44-1334 463826; E-mail: eli.zysman-colman@st-andrews.ac.uk;

URL: <http://www.zysman-colman.com>

^bCEISAM UMR CNRS 6230, Université de Nantes, 2 rue de la Houssinière, BP 92208, 44322 Nantes Cedex 3, France

^cSchool of chemistry, University of Leeds, Woodhouse Lane, Leeds, LS2 9JT, UK

SUPPORTING INFORMATION

Table of Contents:

	Pages
Experimental section	S3
¹ H NMR and ¹ H DOSY NMR spectra	S4
Calculation of hydrodynamic radii (r_s)	S5
HR-ESI-MS characterization	S6
X-ray crystallography	S9
Optoelectronic characterization	S12
Computational investigations	S15
References	S16

Experimental section.

General Synthetic Procedures. Commercial chemicals were used as supplied. All reactions in the synthesis of the ligands and cages were performed using standard Schlenk techniques under inert (N_2) atmosphere with reagent-grade solvents. Flash column chromatography was performed using silica gel (Silia-P from Silicycle, 60 Å, 40-63 μm). Analytical thin layer chromatography (TLC) was performed with silica plates with aluminum backings (250 μm with indicator F-254). Compounds were visualized under UV light. 1H (including 1H DOSY), and ^{13}C solution-phase NMR spectra were recorded on a Bruker Avance spectrometer operating at 11.7 T (Larmor frequencies of 500, 126 and 471 MHz, respectively). The following abbreviations have been used for multiplicity assignments: “s” for singlet, “d” for doublet, “t” for triplet, “m” for multiplet and “br” for broad. Melting points (Mps) were recorded using open-ended capillaries on an Electrothermal melting point apparatus and are uncorrected. High-resolution mass spectra of **Ruqpy** was recorded at the EPSRC UK National Mass Spectrometry Facility at Swansea University on a quadrupole time-of-flight (ESI-Q-TOF), model ABSciex 5600 Triple TOF in positive electrospray or nanospray ionization mode and spectra were recorded using sodium formate solution as the calibrant. HR-ESI mass spectra of cage **RuPd** was recorded at the University of Leeds on a Bruker MaXis Impact instrument in positive ion mode. The samples were injected by direct infusion from DMSO solutions of concentration of ca. 1×10^{-4} M. The syntheses of **Ruqpy** follow previously reported methods.¹

General procedure for the synthesis of cage RuPd. In a dry 10 mL Schlenk vial, ligands **Ruqpy** (2 equiv.) and $[Pd(NCMe)_4](BF_4)_2$ (1 equiv.) were dissolved in $DMSO-d_6$ (1 mL) to give a concentration of the ligands of approximately 0.05 M. The solution was degassed for five minutes by bubbling nitrogen and heated at 85 °C for 12 h under a nitrogen atmosphere. The solution was

cooled to room temperature and the black solid was filtered through celite. A 2M MeOH/H₂O solution (1:1 v/v) of NH₄PF₆ (5 mL) was added to the resulting DMSO solution and the mixture was stirred at room temperature for 4h. The solution was cooled in an ice bath for 30 minutes and the obtained precipitate was filtered, washed with water and diethyl ether and dried under vacuum affording a dark red solid.

[Pd₄(Ruqpy)₈](PF₄)₂₄, (RuPd): Yield: 92%. Mp: 310 - 315°C (degraded). ¹H NMR (500 MHz, DMSO-*d*₆) δ (ppm): δ 9.63 (bd, 16H), 8.96 (bd, 8H), 8.88 – 8.81 (m, 18H), 8.25 (bs, 18H), 7.91 – 7.82 (m, 18H), 7.56 – 7.45 (m, 18H), 1.40 – 1.42 (m, 288H). ¹⁹F NMR {PF₆⁻} (417 MHz, CD₂Cl₂) δ (ppm): -69.38 (s), -70.86 (s). **HR ESIMS: [M-BF₄]⁺ Calculated:**
[(C₅₆H₆₂N₈Ru)₈Pd₄(BF₄)₁₈(H₂O)₂]⁶⁺: 1601.6724 **Found:** 1601.6721;
[(C₅₆H₆₂N₈Ru)₈Pd₄(BF₄)₁₇(H₂O)₂]⁷⁺: 1360.4329 **Found:** 1360.4390;
[(C₅₆H₆₂N₈Ru)₈Pd₄(BF₄)₁₆(H₂O)₂]⁸⁺: 1179.5033 **Found:** 1179.5078.

¹H NMR and ¹H DOSY NMR of Ruqpy and RuPd.

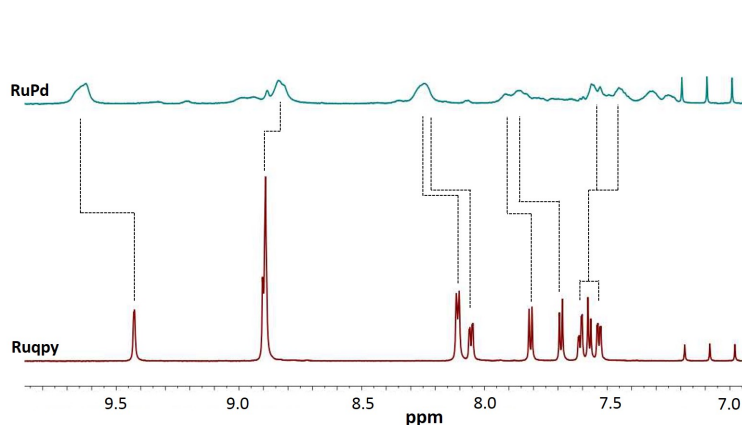


Figure S1. ¹H NMR spectrum of **Ruqpy** (in red) and cage **RuPd** (in light-blue) collected in DMSO-*d*₆ at 298 K.

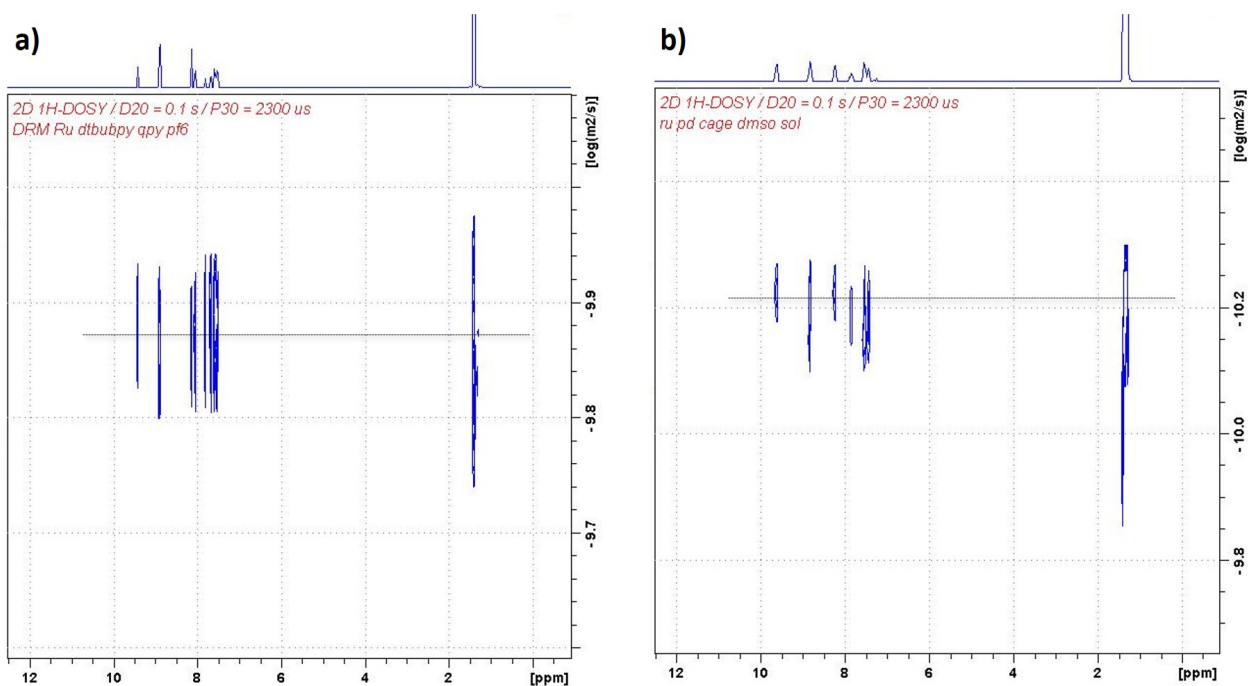


Figure S2. ^1H DOSY NMR spectrum of: **a) Ruqpy** ($D = 1.3 \times 10^{-10} \text{ m}^2/\text{s}$); **b) RuPd** ($D = 5.3 \times 10^{-11} \text{ m}^2/\text{s}$). The spectra were collected in $\text{DMSO-}d_6$ at 298 K.

Calculation of Hydrodynamic Radii (r_s) of Ruqpy and RuPd

Table S1. Comparison of diffusion coefficients (D , $\text{m}^2 \text{s}^{-1}$) of ligand and cage obtained by ^1H DOSY NMR (500 MHz, $\text{DMSO-}d_6$).

ligand	D metalloligand ($\text{m}^2 \text{s}^{-1}$)	cage	D cage ($\text{m}^2 \text{s}^{-1}$)	r_s ligand (nm)	r_s cage (nm)
Ruqpy	1.3×10^{-10}	4PyCzBP-Pd	5.3×10^{-11}	0.83	1.97

In diffusion experiments, the molecular size of the ligand and metallocage are estimated by the Stokes-Einstein equation:

$$r_s = \frac{k_b \cdot T}{6\pi \cdot \eta \cdot D}$$

With r_s = hydrodynamic or Stokes radii of the ligands or metallogage, which are assumed to exhibit a spherical shape, k_b = Boltzmann constant, T = temperature (298 K), η = viscosity of DMSO solution (1.99 mPa · s) and D = diffusion coefficient, obtained here by ^1H DOSY NMR.

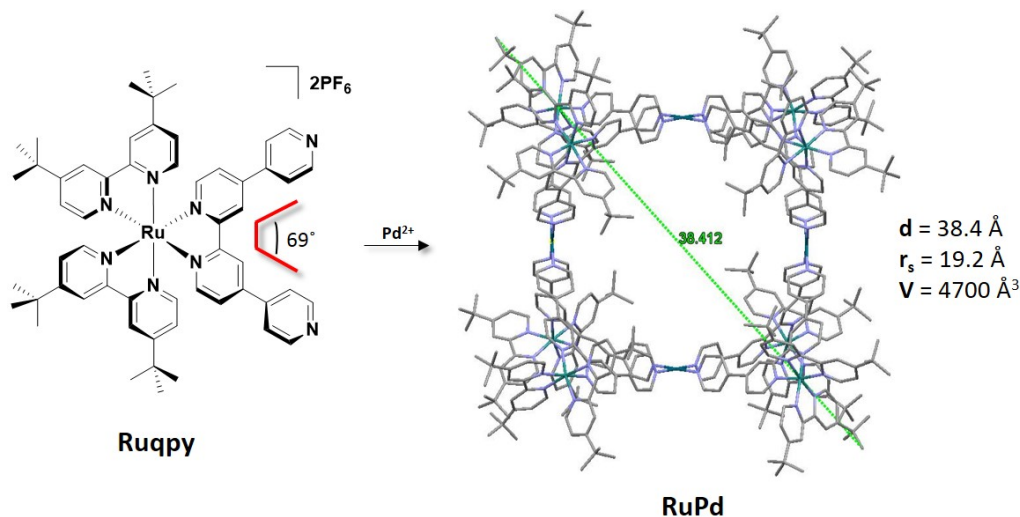


Figure S3. Illustration of the coordinating vector of **Ruqpy** and of the long diagonal distance between opposite t-butyl groups of cage **RuPd**. The structures of **RuPd** was obtained by X-ray single crystal diffraction.

HR-ESI-MS of Ruqpy and RuPd.

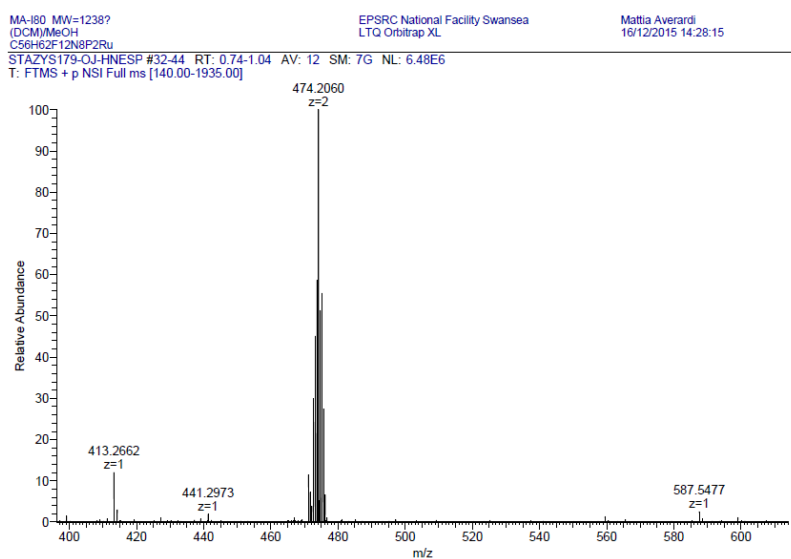


Figure S4. HR-MS spectra of $[\text{Ru}(\text{dtBubpy})_2(\text{qpy})](\text{PF}_6)_2$, **Ruqpy**.

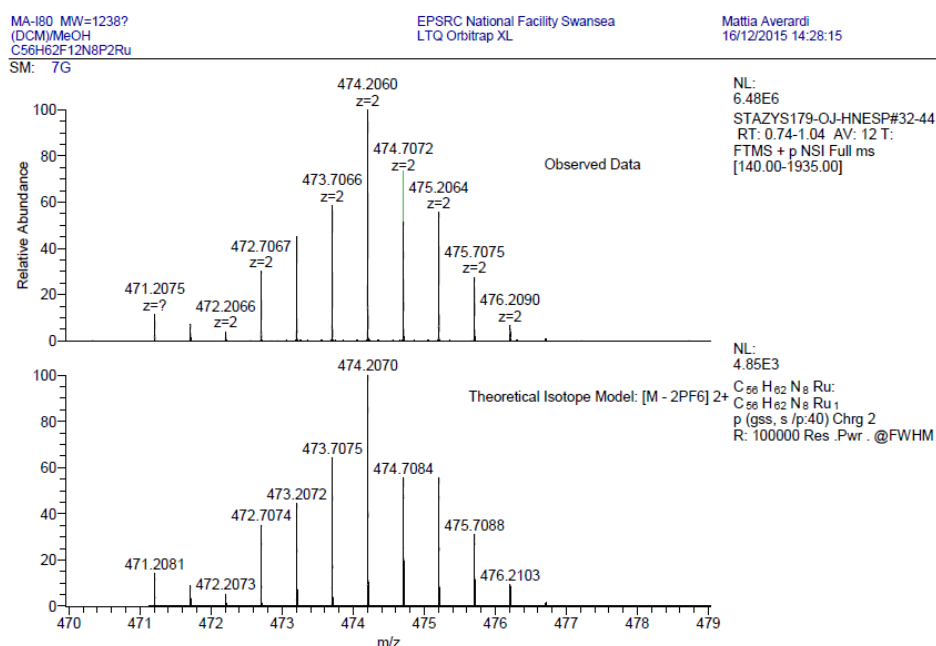


Figure S5. Molecular ion of HR-MS spectrum of $[\text{Ru}(\text{dtBubpy})_2(\text{qpy})](\text{PF}_6)_2$, **Ruqpy**.

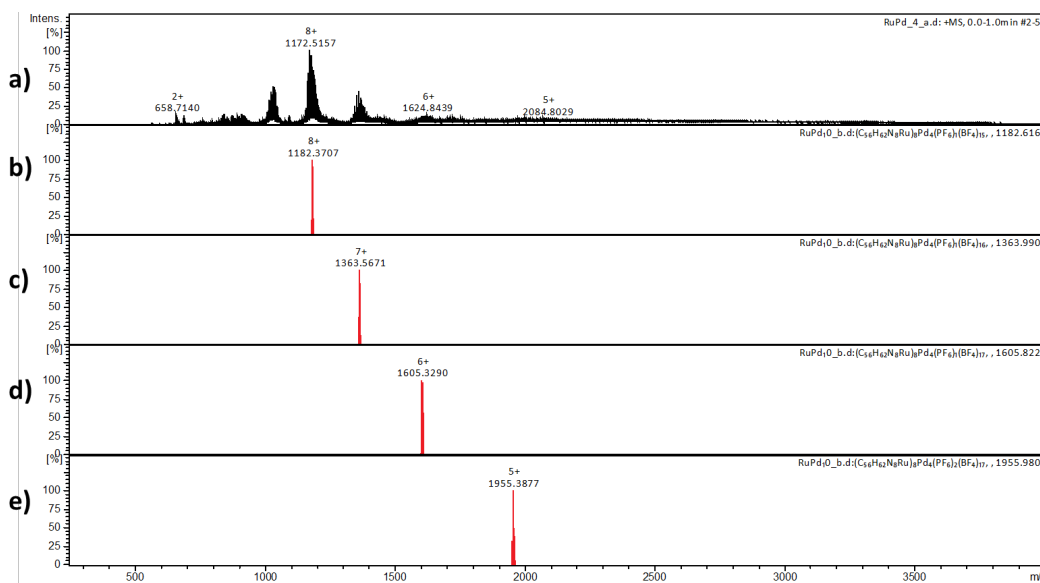


Figure S6. a) ESI-MS spectra of **RuPd**. Simulated MS spectra of: b) $[(\text{RuPd})-(\text{BF}_4)_8]^{8+}$; c) $[(\text{RuPd})-(\text{BF}_4)_7]^{7+}$; d) $[(\text{RuPd})-(\text{BF}_4)_6]^{6+}$; e) $[(\text{RuPd})-(\text{BF}_4)_5]^{5+}$.

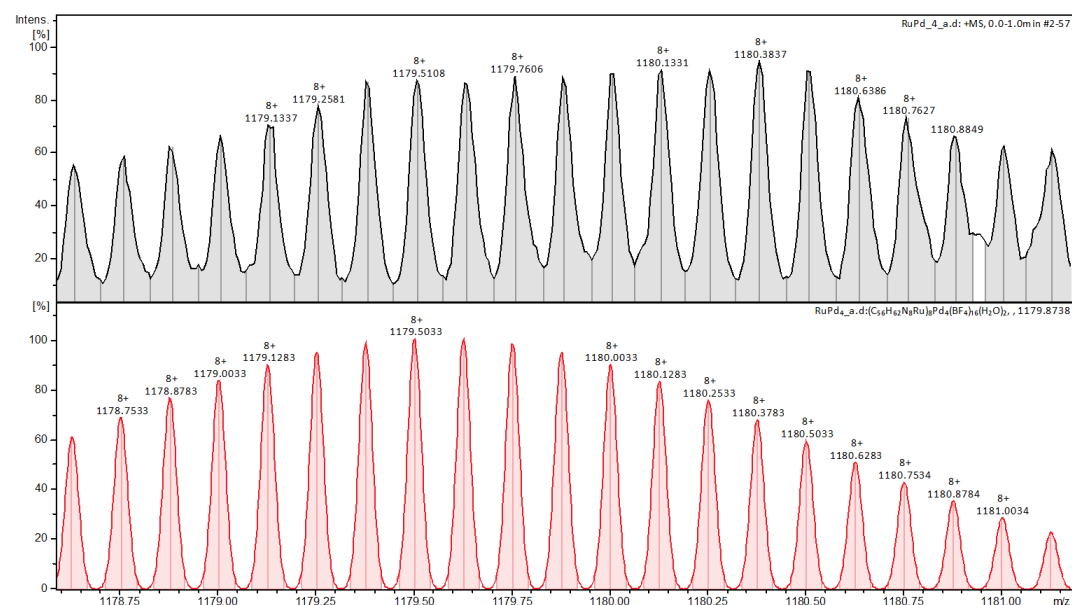


Figure S7. ESI-MS spectra of the $[(\text{RuPd})-(\text{BF}_4)_8]^{8+}$ of **RuPd** (in black) and simulation of isotopic distribution pattern of $[(\text{RuPd})-(\text{BF}_4)_8]^{8+}$ (in red).

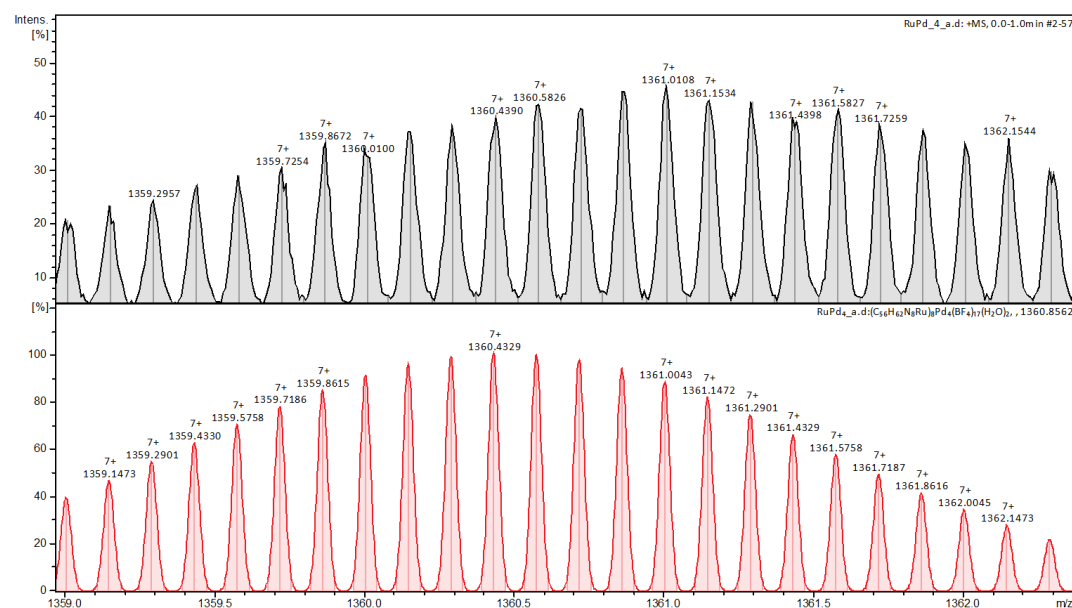


Figure S8. ESI-MS spectra of the $[(\text{RuPd})-(\text{BF}_4)_7]^{7+}$ of **RuPd** (in black) and simulation of isotopic distribution pattern of $[(\text{RuPd})-(\text{BF}_4)_7]^{7+}$ (in red).

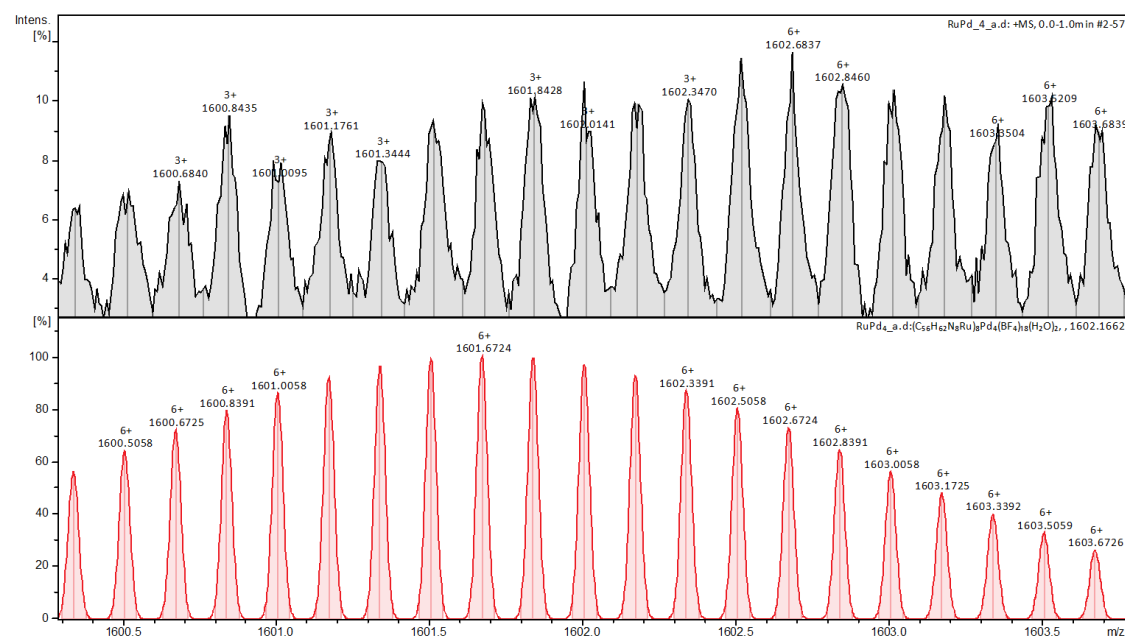


Figure S9. ESI-MS spectra of the $[(\text{RuPd})-(\text{BF}_4)_6]^{6+}$ of **RuPd** (in black) and simulation of isotopic distribution pattern of $[(\text{RuPd})-(\text{BF}_4)_6]^{6+}$ (in red).

X-ray crystallography

Crystals of **Ruqpy** (as the monoprotonated $[\text{RuqpyH}]\text{PF}_6$, Figure S10) were grown by the vapour-diffusion of diethyl ether into a CH_2Cl_2 solution of **Ruqpy**, while crystals of **RuPd** were grown by the vapour-diffusion of a 1:1 mixture of ethyl acetate-hexane into a DMSO solution of **RuPd**. X-ray diffraction data for both **RuPd** and **Ruqpy** were collected by using a Rigaku MM-007HF High Brilliance RA generator/confocal optics and XtaLAB P100 or P200 system, with Cu $K\alpha$ radiation ($\lambda = 1.54187 \text{ \AA}$). Intensity data were collected at low temperature (125 K for **Ruqpy**, 173 K for **RuPd**) using either ω , or both ω and ϕ steps, accumulating area detector images spanning at least a hemisphere of reciprocal space. All data were corrected for Lorentz polarization effects. A multiscan absorption correction was applied by using CrysAlisPro.² Structures were solved by intrinsic phasing methods (SHELXT)³ and refined by full-matrix least-squares against F^2 (SHELXL-2016/6).⁴ Non-hydrogen atoms were refined anisotropically, and carbon-bound hydrogen

atoms were refined using a riding model. Hydrogen atoms bound to nitrogen in **[RuqpyH]PF₆** were located from the difference Fourier map and refined with their thermal parameter riding on that of the parent nitrogen, and subject to distance restraints. All calculations were performed using the CrystalStructure⁵ interface. **[RuqpyH]PF₆** was partially protonated at both external pyridine nitrogens, and the PF₆⁻ anion balancing this charge was disordered over two sites. A variety of crystallographic restraints were required for the PF₆⁻ anions. All crystals of **RuPd** tried showed extremely weak diffraction at higher angles, indicative of the large void-spaces and poor ordering of solvent molecules and anions. These voids led to relatively poor ordering of large parts of the **RuPd** cage, particularly the 4,4'-di-*tert*-butyl-2,2'-bipyridines, and consequently in large thermal motion across most of the cage. A variety of crystallographic constraints and restraints were required within the structural model. Both structures showed void-spaces in which nothing chemically sensible could be modelled, so the PLATON SQUEEZE⁶ routine was used to model this disordered electron density. In the case of **RuPd**, this diffuse electron density would also have contained twenty disordered PF₆⁻ per cage (2.5 per asymmetric unit). The formula of the **RuPd** cage includes these un-ordered anions (and they are correspondingly included in calculated values of ρ , μ , and F(000)), but the unknown solvent is not accounted for in the formula of either structure. Selected crystallographic data are presented in Table S2. CCDC 1828574 and 1828575 contains the supplementary crystallographic data for this paper. The data can be obtained free of charge from The Cambridge Crystallographic Data Centre via www.ccdc.cam.ac.uk/structures.

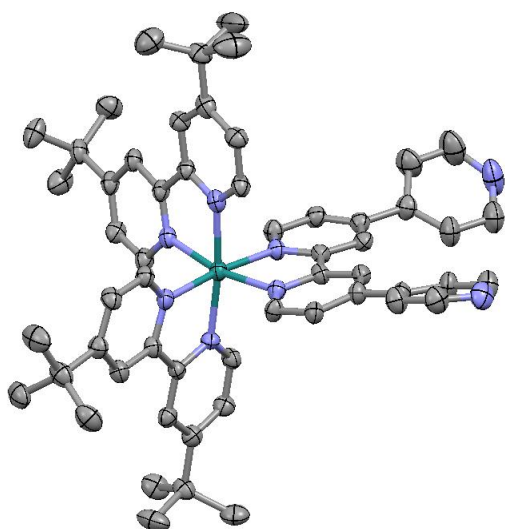


Figure S10. X-ray crystal structure of $[\text{Ru}(\text{dtBubpy})_2(\text{qpyH})](\text{PF}_6)_3$, $[\text{RuqpyH}]\text{PF}_6$. Ellipsoids are drawn at the 50 % probability level. Solvent molecules, hydrogen atoms and PF_6 counterions are omitted for clarity.

Table S2. Selected crystallographic data.

	[RuqpyH]PF₆	RuPd
empirical formula	C ₅₆ H ₆₃ F ₁₈ N ₈ P ₃ Ru	C ₄₄₈ H ₄₉₆ F ₁₄₄ N ₆₄ P ₂₄ Pd ₄ Ru ₈
fw	1384.13	11490.58
crystal description	red plate	red plate
crystal size [mm ³]	0.03×0.03×0.02	0.09×0.07×0.01
crystal system	tetragonal	tetragonal
space group	$I\bar{4}$	$P4/mnc$
<i>a</i> [Å]	24.99060(14)	26.7344(7)
<i>c</i> [Å]	20.6467(2)	51.852(2)
vol [Å ³]	12894.49(16)	37060(2)
<i>Z</i>	8	2
ρ (calc) [g/cm ³]	1.426	1.030
μ [mm ⁻¹]	3.513	3.203
F(000)	5648	11648
reflns collected	77082	370005
independent reflns (<i>R</i> _{int})	13042 (0.0545)	17665 (0.5638)
data/restraints/ params	13042/300/855	17657/1025/597
GOF on <i>F</i> ²	1.047	1.260
<i>R</i> ₁ [<i>I</i> > 2σ(<i>I</i>)]	0.0664	0.1203
<i>wR</i> ₂ (all data)	0.1906	0.3675
largest diff. peak/hole [e/Å ³]	1.22, -0.62	0.53, -0.44

Optoelectronic Characterization.

Photophysical measurements. All samples were prepared in HPLC grade CH_2Cl_2 or DMSO with varying concentrations on the order of 10^{-4} - 10^{-6} M. Absorption spectra were recorded at room temperature using a Shimadzu UV-1800 double beam spectrophotometer. Molar absorptivity determination was verified by linear least-squares fit of the values obtained from at least four independent solutions at varying concentrations with absorbance ranging from 6.05×10^{-5} to 2.07×10^{-5} M.

The sample solutions for the emission spectra were prepared in HPLC-grade DCM and degassed *via* freeze-pump-thaw cycles using a quartz cuvette designed in-house. Steady-state emission and excitation spectra and time-resolved emission spectra were recorded at 298 K using an Edinburgh Instruments F980. All samples for steady-state measurements were excited at 360 nm or 555 nm using a xenon lamp, while samples for time-resolved measurements were excited at 378 nm using a PDL 800-D pulsed diode laser. Photoluminescence quantum yields were determined using the optically dilute method.⁷ A stock solution with absorbance of *ca.* 0.5 was prepared and then four dilutions were prepared with dilution factors between 2 and 20 to obtain solutions with absorbances of *ca.* 0.095, 0.065, 0.05 and 0.018, respectively. The Beer-Lambert law was found to be linear at the concentrations of these solutions. The emission spectra were then measured after the solutions were rigorously degassed *via* three freeze-pump-thaw cycles prior to spectrum acquisition. For each sample, linearity between absorption and emission intensity was verified through linear regression analysis and additional measurements were acquired until the Pearson regression factor (R^2) for the linear fit of the data set surpassed 0.9. Individual relative quantum yield values were calculated for each solution and the values reported represent the slope value. The equation $\Phi_s =$

$\Phi_r(A_r/A_s)(I_s/I_r)(n_s/n_r)^2$ was used to calculate the relative quantum yield of each of the sample, where Φ_r is the absolute quantum yield of the reference, n is the refractive index of the solvent, A is the absorbance at the excitation wavelength, and I is the integrated area under the corrected emission curve. The subscripts s and r refer to the sample and reference, respectively. A solution of quinine sulfate in 0.5 M H_2SO_4 ($\Phi_r = 54.6\%$) was used as external reference.⁸

UV-Vis spectroscopy (DCM solution).

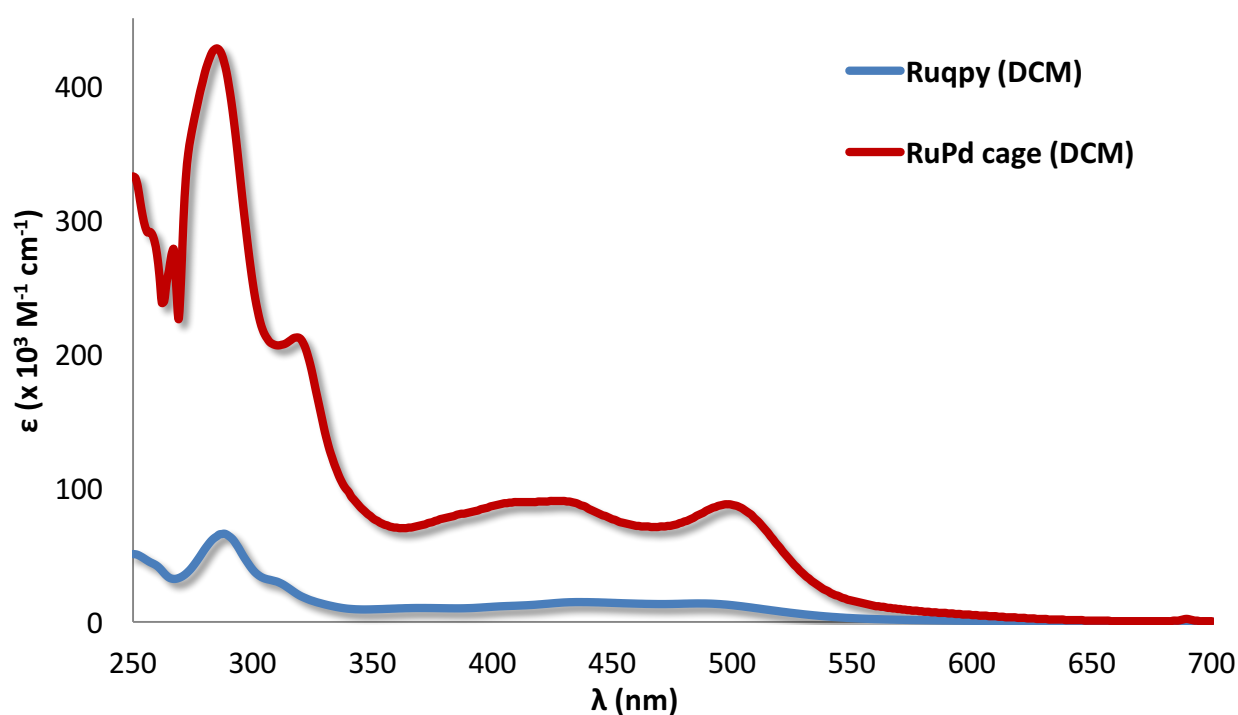


Figure S11. UV-Vis spectra of **Ruqpy** (light-blue line) and cage **RuPd** (red line) collected in CD_2Cl_2 at 298 K.

Table S3. UV-Vis absorptions of **Ruqpy** and **RuPd**

Compound	λ_{max}^a (nm)
	$[\epsilon (\times 10^3 \text{ M}^{-1} \text{ cm}^{-1})]$
Ruqpy	289 [65.5], 311 [29.6], 373 [10.7], 437 [15.1], 492 [13.9]
RuPd	287 [426.3], 320 [212.1], 408 [89.1], 436 [86.7], 505 [85.02]

^a UV-Vis absorption in DCM with a concentration in the order of 10^{-5} – 10^{-6} M collected at 298 K.

Computational Investigations.

All calculations are based on Density Functional Theory (DFT). The geometries of the complexes were fully optimized in the gas phase using the B3LYP functional⁹ in combination with the 6-31G(d) basis set for the light atoms. Scalar relativistic effects were included for the Ru and Pd atoms by using the LANL2DZ pseudopotentials.¹⁰ The so-called *superfinegrid* was used to ensure numerically stable results, and point group symmetry (C_{4h}) was used to lighten the computational burden. All calculations were carried out with the Gaussian09.D01 and Gaussian16.A.03 program packages.¹¹

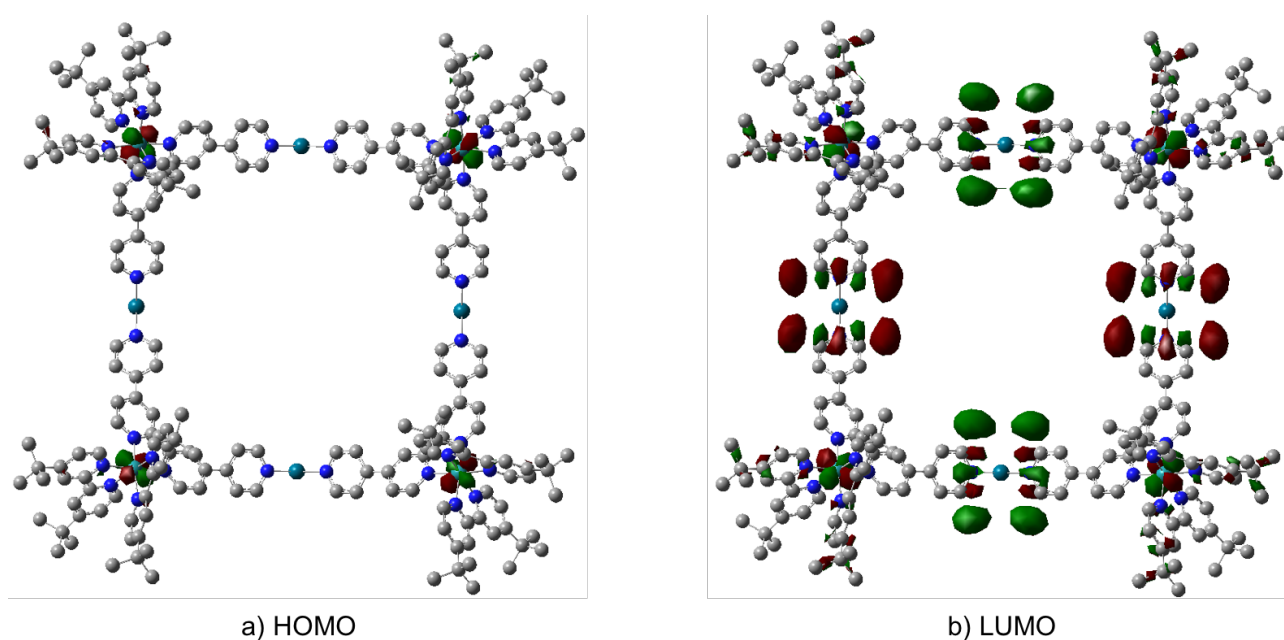


Figure S12. HOMO (a) and LUMO (b) orbitals ((B3LYP/6-31G(d))) of the **RuPd** cage. Hydrogen atoms omitted for clarity

References

- (1). D. Rota Martir, M. Averardi, D. Escudero, D. Jacquemin and E. Zysman-Colman, *Dalton Trans.*, 2017, **46**, 2255-2262.
- (2). *CrysAlisPro v1.171.38.43i or v1.171.39.8d*, Rigaku Oxford Diffraction, Rigaku Corporation, Oxford, U.K., 2015.
- (3). G. Sheldrick, *Acta Crystallogr., Sect. A*, 2015, **71**, 3-8.
- (4). G. Sheldrick, *Acta Crystallogr., Sect. C: Cryst. Struct. Commun.*, 2015, **71**, 3-8.
- (5). *CrystalStructure v4.2.*, The Woodlands, Texas, USA and Rigaku Corporation, Tokyo, Japan, 2015.
- (6). A. Spek, *Acta Crystallogr., Sect. C: Cryst. Struct. Commun.*, 2015, **71**, 9-18.
- (7). G. A. Crosby and J. N. Demas, *J. Phys. Chem.*, 1971, **75**, 991-1024.
- (8). W. H. Melhuish, *J. Phys. Chem.*, 1961, **65**, 229-235.
- (9). (a) A. D. Becke, *J. Chem. Phys.*, 1993, **98**, 5648; (b) C. Lee, W. Yang and R. G. Parr, *Phys. Rev. B*, 1988, **37**, 785-789.
- (10). (a) P. J. Hay and W. R. Wadt, *J. Chem. Phys.*, 1985, **82**, 299-310; (b) L. E. Roy, P. J. Hay and R. L. Martin, *J. Chem. Theory Comput.*, 2008, **4**, 1029-1031; (c) A. W. Ehlers, M. Böhme, S. Dapprich, A. Gobbi, A. Höllwarth, V. Jonas, K. F. Köhler, R. Stegmann, A. Veldkamp and G. Frenking, *Chem. Phys. Lett.*, 1993, **208**, 111-114.
- (11). (a) M. J. Frisch, G. W. Trucks, H. B. Schlegel, G. E. Scuseria, M. A. Robb, J. R. Cheeseman, G. Scalmani, V. Barone, B. Mennucci, G. A. Petersson, H. Nakatsuji, M. Caricato, X. Li, H. P. Hratchian, A. F. Izmaylov, J. Bloino, G. Zheng, J. L. Sonnenberg, M. Hada, M. Ehara, K. Toyota, R. Fukuda, J. Hasegawa, M. Ishida, T. Nakajima, Y. Honda, O. Kitao, H. Nakai, T. Vreven, J. A. Montgomery Jr., J. E. Peralta, F. Ogliaro, M. Bearpark, J. J. Heyd, E. Brothers, K. N. Kudin, V. N. Staroverov, R. Kobayashi, J. Normand, K. Raghavachari, A. Rendell, J. C. Burant, S. S. Iyengar, J. Tomasi, M. Cossi, N. Rega, J. M. Millam, M. Klene, J. E. Knox, J. B. Cross, V. Bakken, C. Adamo, J. Jaramillo, R. Gomperts, R. E. Stratmann, O. Yazyev, A. J. Austin, R. Cammi, C. Pomelli, J. W. Ochterski, R. L. Martin, K. Morokuma, V. G. Zakrzewski, G. A. Voth, P. Salvador, J. J. Dannenberg, S. Dapprich, A. D. Daniels, Ö. Farkas, J. B. Foresman, J. V. Ortiz, J. Cioslowski and D. J. Fox, Gaussian Inc., Wallingford, CT, 2013. ; (b) M. J. Frisch, G. W. Trucks, H. B. Schlegel, G. E. Scuseria, M. A. Robb, J. R. Cheeseman, G. Scalmani, V. Barone, G. A. Petersson, H. Nakatsuji, X. Li, M. Caricato, A. V. Marenich, J. Bloino, B. G. Janesko, R. Gomperts, B. Mennucci, H. P. Hratchian, J. V. Ortiz, A. F. Izmaylov, J. L. Sonnenberg, Williams, F. Ding, F. Lipparini, F. Egidi, J. Goings, B. Peng, A. Petrone, T. Henderson, D. Ranasinghe, V. G. Zakrzewski, J. Gao, N. Rega, G. Zheng, W. Liang, M. Hada, M. Ehara, K. Toyota, R. Fukuda, J. Hasegawa, M. Ishida, T. Nakajima, Y. Honda, O. Kitao, H. Nakai, T. Vreven, K. Throssell, J. A. Montgomery Jr., J. E. Peralta, F. Ogliaro, M. J. Bearpark, J. J. Heyd, E. N. Brothers, K. N. Kudin, V. N. Staroverov, T. A. Keith, R. Kobayashi, J. Normand, K. Raghavachari, A. P. Rendell, J. C. Burant, S. S. Iyengar, J. Tomasi, M. Cossi, J. M. Millam, M. Klene, C. Adamo, R. Cammi, J. W. Ochterski, R. L. Martin, K. Morokuma, O. Farkas, J. B. Foresman and D. J. Fox, Wallingford, CT, 2016.